Field emission image analysis: Precise determination of emission site density and other parameters

Rajkumar Patra[1*], Anjali Singh[2], V. D. Vankar[3], S. Ghosh[3]

[1]*Material Systems for Nanoelectronics, Technische Universität Chemnitz, Chemnitz, 09107, Germany*
[2]*Theoretical Sciences Unit, Jawaharlal Nehru Centre for Advanced Scientific Research, Jakkur, Bangalore 560064, India*
[3]*Nanotech Laboratory, Indian Institute of Technology Delhi, Hauz Khas, New Delhi 110016, India*

[*]Corresponding author. E-mail: rajkumar.patra@etit.tu-chemnitz.de

ABSTRACT

We report a simple and detailed simulation based analysis of an experimental field emission (FE) image captured on a phosphor coated indium tin oxide (ITO)/glass plate due to the electron emission from a multiwalled carbon nanotube (MWCNT) film. Emission intensity versus effective emissive area, number of CNTs present in the film contributing emission process and number density of MWCNTs at high field (during FE process) along with other FE parameters *viz.* turn on field, threshold field are determined, which agrees well with experimental results. Over estimation of calculated value over experimental results is realized with creation of new emission sites at high electric field due to combined effect of divergence of electron within electrode because of electron-air molecule collision, assumption of evenly placement of emitters during calculation, damages and/or tear-off of emitters at high electric field, contribution of adsorbates of MWCNT walls and the energy loss due to absorption of phosphor atom. This analysis renders a unique way to analyze field emission data and supports the theoretical formulation to evaluate the best possible values of FE parameters. Copyright © 2016 VBRI Press.

Keywords: Field emission; image processing; carbon nanotube.

Introduction

The electron field emission (FE) is an emerging technique for the next generation display technology, field emission based sources for microscopy and next generation X-ray, microwave sources [1-3]. The most important advantage of this type of display is that, it consumes relatively less power as compared to the existing one. The important characteristics of an electron field emitter are emission current density, turn-on electric field, field enhancement factor etc [4]. With the advancement of carbon nanotubes and various composites [5-11], FE studies receive a strong support to establish it in the field of display technology and cold cathode sources. Although various experimental and theoretical works on field emission have been reported [4,5,12-14] to understand FE process, the extraction of the important FE parameters remains a challenging issue till date because of complex structure and the properties of field emission materials. The general approach to determine these parameters is to plot current density versus electric field from experimentally obtained data and fit this with an appropriate theoretical model. In many cases, Fowler-Nordhein (F-N) equation [4, 12] can be used as the theoretical fit to the experimental data and to extract the parameters. However, for other nanomaterials like CNTs, CNT-composites, nanodimensional oxides, carbides, borides etc. it is difficult to find a universal equation to fit the experimental data. The problems generally arise due to lack of knowledge related to the exact number of active

emission sites, their spatial distribution and the effective emissive area of a FE cathode. Incorporation of this information in the appropriate theoretical equation is must for evaluation of the parameters with best possible accuracy. Recently, Forbes [15] showed the same discrepancy between the theoretical and experimental data and got best possible fit by introducing some additional parameters in standard F-N equations. Although FE parameters were extracted theoretically by fitting experimental data, there is no direct method of extracting those parameters more accurately. However, to get the information about number of emission sites and effective emissive area by any experimental technique and extrapolation of theoretical models are rarely studied. In 2005, Lysenkov *et al.* [16] reported estimation of emitter sites in an Integral Measurement system with Luminescent Screen (IMLS) where luminescence screen, field emission scanning microscope (FESM), photo multiplier are integrated together in FE set up. In this study, mapping of FE current with respect to voltage along with image formed in the luminescent screen and FESM images were combined together to get an idea of contribution from individual emitter. A detailed image analysis was not performed.

Therefore, our main objectives are (i) to measure effective emissive area during field emission process, (ii) to determine the number of active emitters takes part in emission process and (iii) to realize more realistic

theoretical model with effective emissive area and number density of active emitters to explain the experimental FE results. In this work, we have taken a simple novel approach to obtain emitter site density, contributing FE images on the phosphor screen (anode) based on a detailed analysis of the image without integrating FESM or any other costly equipment. The FE parameter determined by this image analysis process, agrees well with the actual experimental value obtained from scanning electron image of the sample and also with the result reported by Lysenkov *et al*. The determination of effective emissive area, the uniformity of the emission during FE process and active emitter density of the MWCNT sample with a very simple cost-effective approach justifies the uniqueness of this work.

Experimental

Materials

The nano-phosphor is synthesized by chemical precipitation method using Zinc Acetate [Company Name: Glaxo Laboratories (India) Ltd., Place of Manufacture: Mumbai, India, Assay:≥98.5%] and Sodium Hydroxide [Company Name: E-Merck (India) Ltd., Place of Manufacture: Mumbai, India, Assay: ≥99%] and coated uniformly on indium tin oxide (ITO) coated glass plates [Company Name: Macwin India Company, Place of Manufacture: Delhi, India, Item Code: SE-ITO-001] by spin coating technique after filtering and annealing. The details of phosphor synthesis method and preparation of phosphor anode plate is reported elsewhere [17]. We kept a mixture of ferrocene [Company Name: Spectrum Pvt. Ltd., Place of Manufacture: Mumbai, India, Assay: 98%] and xylene [Company Name: Fisher Scientific, Place of Manufacture: Mumbai, India, Assay: ≥98.5%] solution in 0.02g/ml ratio inside a quartz tube to synthesize multiwalled carbon nanotube (MWCNT) via thermal CVD technique [11].

Method

This phosphor coated ITO-glass plate is placed inside the FE chamber (operated at a pressure 1.0×10^{-7} mbar) and used as anode. The sample (MWCNT film synthesized by microwave plasma enhanced CVD system [18]) is placed and used as cathode. The electrodes are assembled in a FE chamber in diode geometry. The distance between cathode and anode can be varied with a resolution of 5.0 μm using a microcontroller based electronic module [7-11]. A scale is placed just beside the phosphor coated ITO-glass plate to standardize the scale factor in the image. A high resolution CCD camera (ARTCAM 200MI) is mounted on the chamber and focused the probable display area of the nano-phosphor coated on ITO-glass plate. The distance between anode (phosphor coated ITO-glass plate) and the cathode (MWCNT film) is kept fixed at 200 μm and the applied voltage is varied from 350V to 3000V. The optimized image corresponding to a voltage of 2950V is taken for further analysis. The surface morphology of the MWCNT films were examined by scanning electron microscopy (ZEISS EVO 50, operating at 20 kV secondary electrons) in order to determine the actual emitter density on the film surface.

Results and discussion

Approach to FE image analysis

The image of field emission spots generated on phosphor coated ITO glass plate (anode) is recorded through CCD camera. A schematic of the FE setup is shown in **Fig. 1**.
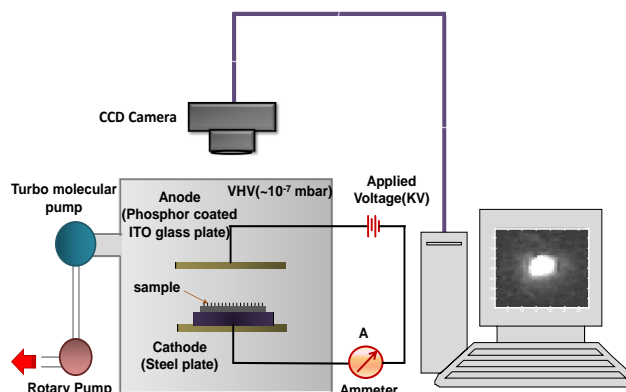

Fig. 1. Schematic of FE set up for capturing FE image using phosphor plate as anode.

Each spot which is due to electron emission from a bunch of active emitters at cathode is analyzed with the help of MATLAB 2010a in the following way. First, the standard scale factor is calculated by measuring the number of pixels for defined distance within the image. The area around a single spot is selected and the pixel value of the grey scale image of the selected area is calculated. This grey scaled image value is plotted along the Z-axis with respective dimensions of the selected area along the X and Y axis. Assuming the pixel value of a grey scale image is proportional to the intensity of that particular pixel, this 3-D plot is designated as the Intensity versus surface plot of the image. Now the projection of the above 3-D plot, *i.e.*, the contour of the intensity variation on the X-Y plane is recorded. Before hitting the phosphor plate, the electrons which are emitted from the emission sites may diverge from their straight line trajectory and hence the contour areas of different fraction (50-100%) of the maximum intensity are obtained. Also, the emission sites can either be evenly placed or randomly placed. For our case, we have chosen the evenly case which is defined by placing each emission site at a separation equal to the diameter of the emitter within the area which is the direct projection (on the cathode) of the image of the selected single spot. Therefore, the maximum number of emitters is packed in a particular contour area of the emission image to obtain the approximate number of the evenly placed emitting sites in that particular contour area. Using this result, the emitter density in that particular spot can also be calculated. The number of emitters and the emitter density calculated at different contour area for different fraction of maximum intensity are plotted and fitted with quadratic equation of contour area. The current density (J) at a particular field (E) is thus directly proportional to the effective emissive area using modified FN equation [19], given by,

$$J = S_r \frac{(a\beta^2 E^2)}{(\varphi t\_y^2)} exp \left(\frac{-bv_y \varphi^{3/2}}{(\beta E)} \right) \tag{1}$$

where, $S_r = \dfrac{\textit{effective emissive area}}{\textit{total area of the sample}}$, E is the applied electric

field, $\beta = \dfrac{E_{local}}{E}$ is the enhancement factor, φ is the work

function of the material, $a = \dfrac{e^2}{8\pi h_p} = 1.54434 \times 10^{-6}$ A.eV.V^{-2},

$b = \dfrac{8\pi}{3} \cdot \dfrac{(2m_e)^{1/2}}{eh_p} = 6.830890 \times 10^9$ eV.V$^{-\frac{3}{2}}$. v.m^{-1} are the constants.

The correction factors [20] are $t_y \approx 1 + \dfrac{1}{9}[y^2 - y^2 \ln y]$

and $v_y \approx 1 - y^2 + \left(\dfrac{1}{3}\right) y^2 \ln y$ where $y = \dfrac{cE^{1/2}}{h}$ and

$c = \left(\dfrac{e^3}{4\pi\varepsilon_0}\right)^{1/2}$ = 1.199985 $eV.V^{1/2}.nm^{1/2}$. The current
density for each contour area is thus calculated and plotted
against the electric field.
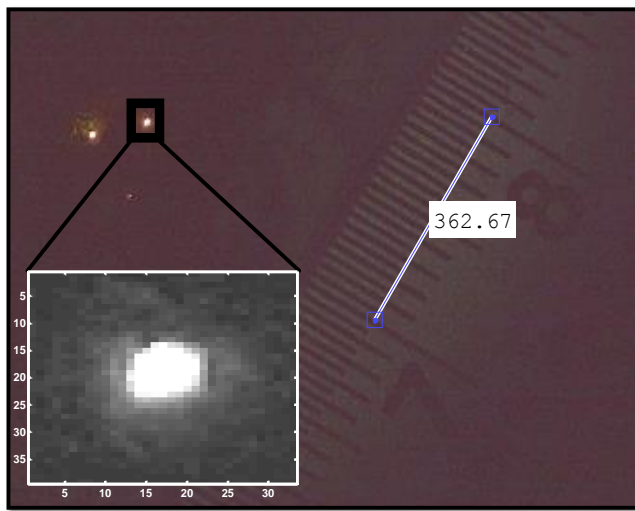
Fig. 2. Electron field emission image taken on nano-phosphor coated
ITO-glass plate and the scale factor. Inset- the cropped image in grey
scale and the line profiling.

*Determination of emitter site density and other FE
parameters*

Electron field emission images due to electron emission
from a MWCNT film on phosphor coated ITO-glass plates
are captured with CCD camera. A typical image is shown in
Fig. 2.

The image captured by the camera has the following
calibration: 10 mm. distances on scale is equivalent to
363.29 pixel distance as indicated in this figure from which
the scale factor is calculated. Among various spots, one of
them (shown in grey in the inset of **Fig. 2**) is selected. The
total area of the cropped image is 1.06 mm^2. A line is
drawn on the cropped image, as shown in **Fig 2 (Inset),** and
the corresponding line profile is obtained for this cropped
image **(Fig. 3(a))**.

This line profile confirms the variation of the intensity
over the line and the uniformity of the intensity over the
spot. In this case, the length of the uniform intensity of the
selected spot is 161.03 μm. The contour plot of the cropped
spot on the surface of the phosphor coated ITO-glass plate
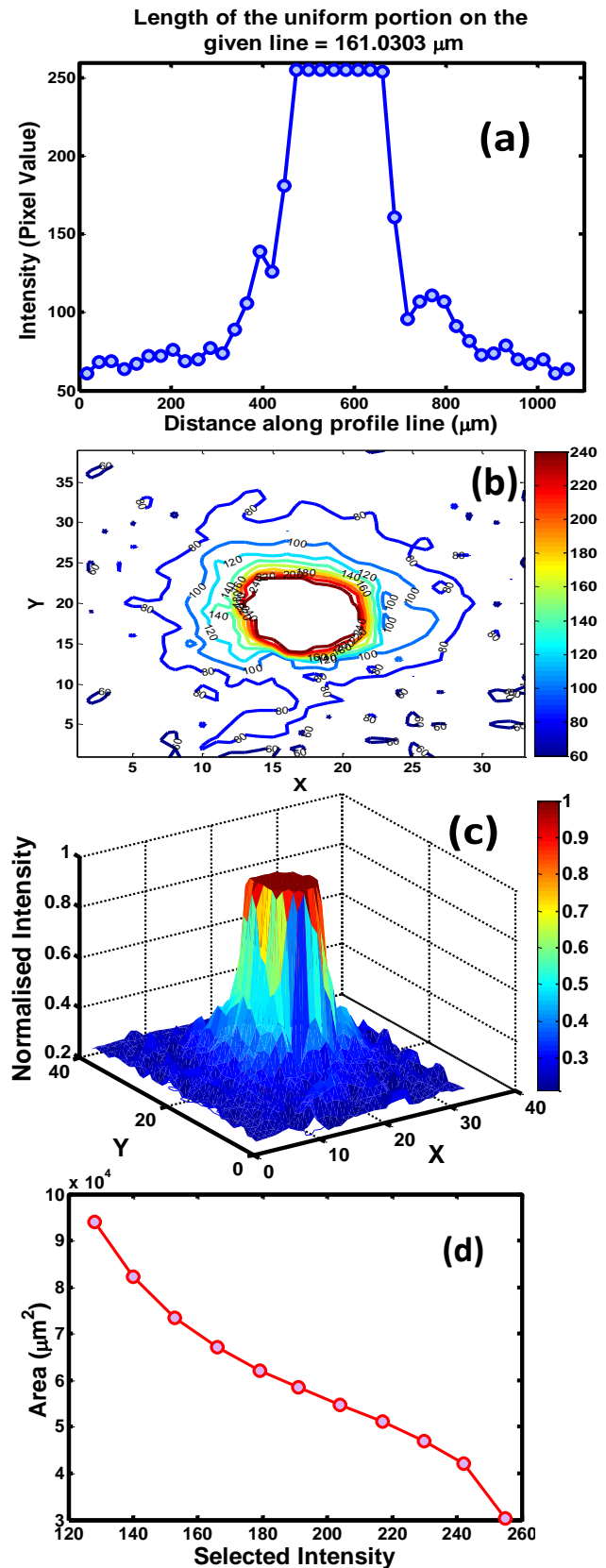is shown in **Fig. 3(b)**.

Fig. 3. (a) The line profile plot of the selected area to calculate the
uniformly illuminated region on phosphor plate. (b) The Contour plot of
the cropped grey scaled image. (c) Surface plot of the cropped grey scaled
image. (d) Selected intensity (fraction of maximum intensity) versus the
effective emissive area plot.

From this plot the intensity variation of the cropped
image over the surface of the phosphor coated ITO-glass

plate can be clearly understood. The surface plot, **Fig. 3(c)**, shows the variation of different intensity regions over the surface of the phosphor plate. Since the electrons emitting from the emission sites can diverge, the area of a particular contour, *i.e.*, the area for a particular fraction of maximum intensity is to be calculated. For an emitter with known radius and known inter-emitter distance, the approximate number of emitter and hence the number density of the emitter within the sample can be found out (assuming the emitters are distributed in same fashion along both X and Y directions) by assuming evenly placing of the emitters. Thus, the number of active emitters within the sample can be approximated. In this work, we have calculated the number of the active emitter and the active emitter density for variation of maximum density from 100% to 50% running this program and found the variation of number density of emitter and the active number of emitters with the emissive area chosen from **Fig. 2**. For any particular selected intensity (fraction of maximum intensity), the respective effective emissive area is calculated. **Fig. 3(d)** shows the variation of effective emissive area with the selected intensity (selected fraction of maximum intensity). From this plot it is clear that, the effective area of the sample increases as the intensity decrease which is quite realistic.
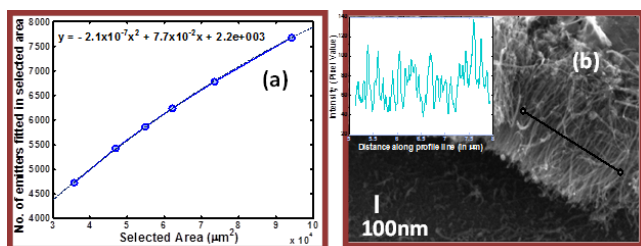

Fig. 4. (a) Number of emitted sites placed in the selected emissive area versus the effective emissive area plot for different selected fraction of maximum intensity with fitting. (b) SEM image and profiling of the actual emitter surface.

The variation of the approximate number of emitters accommodated within a particular area versus the effective emissive area along with the fitting of this variation is shown in **Fig. 4(a)**. The fitting result reveals that the approximate number of emitters (n) placed for the spot size varies quadratically with effective emissive area (A_{eff}) of the sample as,

$$n = pA_{eff}^2 + qA_{eff} + r \tag{2}$$

where, for our case, $p = -2.1 \times 10^{-7}$ μm^{-2}, $q = 7.7 \times 10^{-2}$ μm^{-1}, $r = 2.2 \times 10^3$. The value of p, q and r may vary with the sample. From this analysis one can get a fairly good idea about the number of active emitters in the sample used. The variation of the number density of the active emitters with the effective emissive area is also calculated. The number density of the active emitters at different selected emissive area is found to be constant at 625 emitters per μm^2. By profiling the SEM image **(Fig 4(b))** with the help of MATLAB 2010b, the number density of the emitters within the actual sample is found to be 460 emitters per μm^2.

The mismatch of calculated value at 2900V over experimental result (image captured with SEM when no voltage applied) may due to (i) the divergence of the electron within the path (because of the collision of air molecules and emitted electron as the chamber pressure is not sufficiently low) between emitter tip and phosphor screen which causes over estimation of illuminated area and hence effective emissive area, (ii) the assumption of radius and separation as well as the evenly placement of the emitters within the effective emissive area during emission process as the SEM image depicts that the emitters may be randomly placed, (iii) number of active emitters and the active emitter density was calculated at high electric field which should be different from actual density of the emitters when no bias applied, since at a particular field it is impossible to activate all the emitter although the kinks/bending of the active/inactive or aligned/non-aligned emitters act as new emission site, (iv) During the FE process, at high applied electric field tear-off and damage tips and walls of the emitters along with adsorbate atoms on MWCNT wall adds new active emission sites significantly by creating new emission sites, (v) some part of the electron energy is utilized by the phosphor atoms as absorption energy to go to higher energy level needed for illumination. The last reason reduces the actual illumination area and/or the intensity although other reasons have the opposite effect. Hence, the calculated effective emissive area increases as combined effect which implies that the emitter density at that particular applied electric field, within the active emissive area, also increases in comparison to the emitter density when no electric field applied. Furthermore, the study with random placement of emitters would be more realistic, but it is more complicated and beyond the scope of this study, due to which we couldn't check the validity of random placement result. From our study, we can conclude that number density of the active emitters can be calculated at a high applied electric field (during FE process) *via* the above discussed image processing analysis. This result is approximately accurate and more realistic.
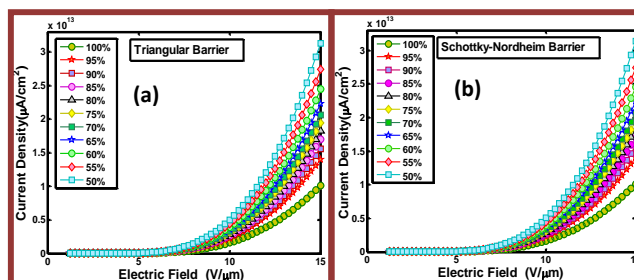

Fig. 5. (a) The J versus E plot for Triangular Barrier for different effective emissive area selected (for selected fraction of maximum intensity). (b) The J versus E plot for Schottky-Nordheim Barrier for different effective emissive area selected (for selected fraction of maximum intensity).

The S_r values are calculated for various A_{eff} and Eqn. (1) is used to calculate the current density (J) from the modified F-N equation **[19]**. The calculated current density corresponding to the effective emissive area (for different fraction of the maximum intensity) for (i) voltage range 350V to 3000V, (ii) enhancement factor 2500 and (iii) distance between anode and cathode 200 μm and the corresponding J-E plot is shown for triangular barrier **[21]** **(Fig. 5(a))** and for schottky-nordheim barrier

[20] (**Fig 5(b)**). Turn on field, V_{to} (defined as the electric field applied when the emission current density is 10μA/cm^2) and threshold field, V_{th} (defined as the electric field applied when the emission current density is 1.0 A/cm^2) are calculated to each case as given in **Fig 5(a)** and **Fig 5(b)**. Calculated turn-on field and threshold field for both triangular barrier and S-N barrier is tabulated in **Table 1**.

Table 1. Threshold Field and Turnon Field at different selected area for Triangular barrier and Schottky-Nordheim barrier.

Selected Intensity (in %)	Turn On Field (V)		Threshold Field (V)	
	Triangular Barrier	Schottky-Nordheim Barrier	Triangular Barrier	Schottky-Nordheim Barrier
50	1.2476	1.2476	2.1056	2.0506
55	1.2477	1.2477	3.8842	3.8258
60	1.2478	1.2478	5.454	5.3933
65	1.2479	1.2479	6.7503	6.688
70	1.248	1.2480	7.8601	7.7978
75	1.2481	1.2481	8.7166	8.6543
80	1.2482	1.2482	9.6371	9.5754
85	1.2483	1.2483	10.6106	10.5500
90	1.2484	1.2484	11.7735	11.7156
95	1.2486	1.2486	13.1556	13.1030
100	1.2492	1.2492	15.8809	15.8619

It is clear from **Table 1** that V_{to} remains almost same; however, V_{th} varies for different A_{eff} (**Fig 6**). We have considered the turon field at 10.0 μA/cm^2 and the threshold field at 1.0 A/cm^2. Hence, the prefactor introduced for S-N barrier has almost no effect on V_{to} (atleast upto the 4th or 5th decimal place) whereas the prefactor effect on V_{th} (as the current density is 10^5 times larger than that for turn-on current density) is notably prominent. We would also like to point out here that the calculation of these fields considering complete sample area is not realistic. To get more realistic V_{to} and V_{th}, the effective emissive area must be considered for such calculation as demonstrated in this study.

$$y = 2 \times 10^{-14}x^3 - 2.6 \times 10^{-9}x^2 - 1.5 \times 10^{-4}x + 22$$
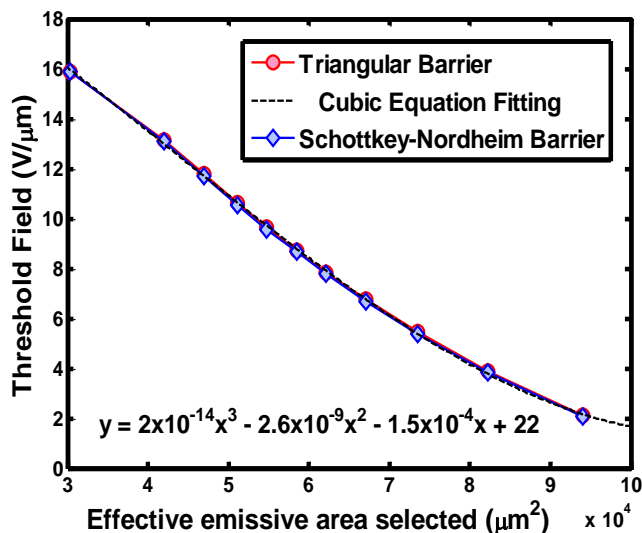
Fig. 6. Threshold field for different selected intensity versus the selected effective emissive area plot for both Triangular barrier and the Schottky-Nordheim Barrier with fitting.

Conclusion

To conclude, we have demonstrated a new, simple approach to estimate the number of active emitters present in a MWCNT film (emission active region) from detailed simulation based analysis of an experimental field emission image. The effective emissive area and the packing density of the active emitters are calculated. Furthermore, the current density at various applied electric field is calculated using the result obtained from image analysis. Other important FE parameters like turn on field and threshold field are also derived from this calculation. This study helps to obtain the FE parameters more accurately despite of any knowledge of the actual number of effective emissive sites or active emitters, from any kind of morphological study during FE process. This also further grants information about uniformity in growth as well as uniformity in emission and the brightness of the image. The knowledge of obtained FE parameters may leads to explore a dense, uniformly distributed active emitter film which is important for high FE current source and high resolution display industry. Furthermore, the mutual interaction between the emitters (with both evenly placed emitters and randomly placed emitters) during the emission process can be envisaged to understand and correlate the basic emission mechanism with experimental result for composite emitter structure.
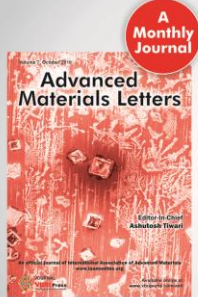
Author's contributions

Conceived the plan: RP, AS, VDV, SG; Performed the expeiriments: RP; Simulation and Data analysis: RP, AS; Wrote the paper: RP, AS, SG, VDV.

References

1. Talin, A. A.; Dean, K.A.; Jaskie, J. E.; Field emission displays: a critical review. *Solid State Electron.* **2001**, *45*, 963.
   DOI: 10.1016/S0038-1101(00)00279-3
2. Tonomura, A.; Komoda, T.; Field emission electron Microscope. *J. Electron Micros.* **1973**, *22*, 141.
3. Jensen, K. L.; Field emitter arrays for plasma and microwave source applications. *Phys. Plasmas.* **1999**, *6*, 2241.
   DOI: 10.1063/1.873502
4. Bonard, J. M.; Salvetat, J. P.; Stöckli, T.; Forr´o, L.; Châtelain, A.; Field emission from carbon nanotubes: perspectives for applications and clues to the emission mechanism. *Appl. Phys. A* **1999**, *69*, 245.
   DOI: 10.1007/s003399900113
5. Lee, N. S.; Chung, D.S.; Han, I.T.; Kang, J.H.; Choi, Y.S.; Kim, H.Y.; Park, S.H.; Jin, Y.W.; Yi, W.K.; Yun, M.J.; Jung, J.E.; Lee, C.J.; You, J.H; Jo, S.H.; Lee, C.G.; Kim, J.M.; Application of carbon nanotubes to field emission displays. *Diam. Relat. Mater.* **2001**, *10*, 265.
   DOI: 10.1016/S0925-9635(00)00478-7
6. Milne, W. I.; Teo, K. B. K; Amaratunga, G. A. J; Legagneux, P.; Gangloff, L.; Schnell, J.P.; Semet, V.; Binh, V. T.; Groening, O.; Carbon nanotube as field emission source. *J. Mater. Chem.* **2004**, *14*, 933.
   DOI: 10.1039/B314155C
7. Patra, R.; Ghosh, S.; Sheremet, E.; Jha, M.; Rodriguez, R. D.; Lehmann, D.; Ganguli, A. K.; Schmidt, H.; Schulze, S.; Hietschold, M.; Zahn, D. R. T.; Schmidt, O. G., Enhanced field emission from lanthanum hexaboride coated multiwalled carbon nanotubes: Correlation with physical properties, *J. Appl. Phys.* **2014**, *116*, 164309.

DOI: 10.1063/1.4898352

8. Patra, R.; Ghosh, S.; Sheremet, E.; Jha, M.; Rodriguez, R. D.; Lehmann, D.; Ganguli, A. K.; Gordan, O. D.; Schmidt, H.; Schulze, S.; Zahn, D. R. T.; Schmidt, O. G., Enhanced field emission from cerium hexaboride coated multiwalled carbon nanotube composite films: A potential material for next generation electron sources, *J. Appl. Phys.* **2014**, *115*, 094302.
   DOI: 10.1063/1.4866990

9. Sarker, D.; Kumar, H.; Patra, R.; Kabiraj, D.; Avasthi, D. K.; K Vayalil, Sarathlal, Roth, S. V.; Srivastava, P.; Ghosh, S., Enhancement in field emission current density of Ni nanoparticles embedded in thin silica matrix by swift heavy ion irradiation, *J. Appl. Phys.* **2014**, *115*, 174304.
   DOI: 10.1063/1.4874435

10. Patra, R.; Sharma, H.; Ghosh, S.; Vankar, V. D.; High Stability Field Emission From Zinc Oxide Coated Multiwalled Carbon Nanotube Film, *Adv. Mat. Lett.* **2013**, *4*, 849.
    DOI: 10.5185/amlett.2013.4465

11. Sreekanth, M.; Ghosh, S.; Patra, R.; Srivastava, P., Highly enhanced and temporally stable field emission from MWCNTs grown on aluminum coated silicon substrate, *AIP Advances*, **2015**, *5*, 067173.
    DOI: 10.1063/1.4923423

12. Fowler, R. H.; Nordheim, L.; Electron Emission in Intense Electric Fields. *P. Roy. Soc. Lond. A.* **1928**, *119*, 173.
    Stable URL: http://www.jstor.org/stable/95023

13. Wei, W.; Jiang, K.; Wei, Y.; Liu, P.; Liu, K.; Zhang, L.; Li, Q.; Fan, S.; LaB$_6$ tip-modified multiwalled carbon nanotube as high quality field emission electron source. *Appl. Phys. Lett.* **2006**, *89*, 203112.
    DOI: 10.1063/1.2388862

14. Khaneja, M.; Singh, S.; Ghosh, S.; Rawat, J. S. B. S.; Chaudhary, P. K.; Kumar, V.; Modeling Field Emission from Single-Tip Carbon Nanotube in Triode Configuration. *Int. J. Green Nanotechnology*. **2012**, *4*, 547.
    DOI: 10.1080/19430892.2012.739061

15. Forbes, R. G.; Extraction of emission parameters for large-area field emitters, using a technically complete Fowler–Nordheim-type equation. *Nanotechnology*. **2012**, *23*, 095706(1).
    DOI: 10.1088/0957-4484/23/9/095706

16. Lysenkov, D.; Müller, G.; Field emission measurement techniques for the optimisation of carbon nanotube cathodes. *Int. J. Nanotechnolog.* **2005**, *2*, 239.
    DOI: 10.1504/IJNT.2005.008062

17. Kataria, V.; *Internal Report*, *M. Tech. Thesis*, Indian Institute of Technology Delhi, **2011**.

18. Sharma, H.; Kaushik, V.; Girdhar, P.; Singh, V.N.; Shukla, A.K.; Vankar, V.D.; Enhanced electron emission from titanium coated multiwalled carbon nanotubes. *Thin Solid Films*. **2010**, *518*, 6915.
    DOI: 10.1016/j.tsf.2010.07.043

19. Gu, G.R.; Li, Y.A.; Ito, T.; Influence of Ti coatings on field emission characteristics of nano-sheet carbon films. *Vacuum.* **2010**, *85*, 531.
    DOI: 10.1016/j.vacuum.2010.09.002

20. Forbes, R. G.; Field emission: New theory for the derivation of emission area from a Fowler-Nordheim plot. *Appl. Phys. Lett.* **2006**, *89*, 113122(1).
    DOI: 10.1063/1.2354582

21. Forbes, R. G.; Simple good approximations for the special elliptic functions in standard Fowler-Nordheim tunneling theory for a Schottky-Nordheim barrier. *J. Vac. Sci. Technol. B.* **1999**, *17*, 526.
    DOI: 10.1116/1.590588